Journal of Nuclear Materials 383 (2008) 34–40

Contents lists available at ScienceDirect

Journal of Nuclear Materials

journal homepage: www.elsevier.com/locate/jnucmat

Microchemical study of high-burnup CANDU® fuel by imaging-XPS

Than Do *, Karen G. Irving, William H. Hocking

Atomic Energy of Canada Limited, Chalk River Laboratories, Chalk River, Ontario, Canada K0J 1J0

ARTICLE INFO

PACS:
81.70
28.41.Bm

ABSTRACT

An advanced facility for characterization of highly radioactive materials by Imaging X-ray Photoelectron Spectroscopy (XPS) has been developed at the Chalk River Laboratories (CRL), based upon over a decade of prior experience with a prototype system. Auxiliary electron and ion guns provide additional *in situ* capabilities for scanning electron microscopy (SEM), scanning Auger microscopy (SAM) and composition depth profiling. The application of this facility to the characterization of irradiated fuel materials will be illustrated with selected results taken from a detailed study of the microchemistry at the fuel-sheath interface in a CANDU fuel element that was irradiated to extended burnup in the NRU (National Research Universal) reactor at CRL. Inside surfaces of the end caps and the welds between the sheath and the end caps as well as the thin-walled Zircaloy-4 sheath were analyzed. The *in situ* SEM capability was essential for selecting different areas on each sample, such as sheath locations with and without a visible retained CANLUB graphite layer, for XPS analysis. Effective infiltration of segregated fission products, especially cesium, into the graphite was demonstrated by depth profiling. A richer chemistry of segregated fission products was found on the end caps than on the sheath with elevated levels of barium, strontium, tellurium, iodine and cadmium as well as cesium. The results are consistent with current understanding of the primary migration route for fission products to the sheath and also indicate that the CANLUB layer functions as a chemical rather than a physical barrier to segregated fission products.

1. Introduction

Because of its exceptional neutron economy, the heavy-water-moderated CANDU reactor has a unique ability to burn natural uranium fuel, but only a modest average burnup is presently achieved. Reliable fuel performance to extended burnup will be essential to fully exploit the additional fuel-cycle flexibility—including slightly enriched uranium (SEU), thoria and mixed uranium-plutonium oxide (MOX) fuels—offered by the CANDU reactor [1]. As any nuclear fuel is burned, many fission products with diverse chemical properties are created [2–5]. Fission products that have limited solubility in the host structure tend to segregate to the fuel grain boundaries from whence they can readily migrate to the fuel sheath [2–8]. The rates of these processes are strongly dependent upon the fuel burnup and operating power as well as the fuel design. Fission-product segregation can be the limiting factor on fuel performance in-reactor and also significantly increases the potential for release of radioactivity from used fuel during subsequent storage or after deep geological disposal [2–4].

The thin-walled Zircaloy-4 sheath used for CANDU fuel, which collapses onto the ceramic fuel pellets under the primary coolant pressure, was initially found to be quite susceptible to stress-corrosion cracking (SCC) [8]. Introduction of the CANLUB graphite coating on the interior surface of the sheath virtually eliminated stress-corrosion cracking problems for the burnup and linear-power ratings achieved with natural uranium fuels in the current generation of CANDU power reactors [8]. The graphite was originally thought to function as a pellet lubricant that would reduce sheath stress; however, the CANLUB layer has been shown to play a more important role as a fission-product chemical barrier [8]. There is also some evidence that the CANLUB layer mediates evolution of the oxygen potential within CANDU fuels [9,10], which in turn may control the chemical speciation and migration of several key fission products [7].

As part of an on-going program to assess the performance of SEU fuels under typical CANDU operating conditions, an experimental fuel bundle was irradiated to extended burnup in the NRU reactor following a moderate power ramp early in life. A detailed study of the microchemistry at the fuel-sheath interface in an intermediate-ring element from this bundle has been conducted by imaging X-ray photoelectron spectroscopy (XPS) and sequential argon-ion sputtering. The inside surface of the weld between the sheath and the end cap as well as representative areas on the sheath and both end caps were composition depth profiled. Appropriate regions were selected for microchemical XPS analysis by *in situ* scanning electron microscopy (SEM).

* Corresponding author.
E-mail addresses: dot@aecl.ca (T. Do), irvingk@aecl.ca (K.G. Irving), hocking-w@aecl.ca (W.H. Hocking).

0022-3115/$ - see front matter Crown Copyright © 2008 Published by Elsevier B.V. All rights reserved.
doi:10.1016/j.jnucmat.2008.08.057

2. Experimental procedures

An experimental fuel bundle was irradiated in the NRU reactor to demonstrate the capability of CANDU fuel to tolerate the conditions expected for slightly enriched uranium (SEU) fuel cycles. The density of the ceramic UO_2 pellets ($l/d = 1$) was 10.5 g/cm^3, the uranium was enriched in ^{235}U to 2.26 wt% and the CANLUB coating on the sheath interior surface was specified to be a minimum of 6 μm thick. Burnup and power varied significantly along the length of the bundle during its early irradiation in a steep neutron-flux gradient, whereas the subsequent irradiation was performed at a central position on the fuel carriage in a nearly uniform neutron flux. A significant power ramp occurred when the bundle was moved to a central position, with ΔP up to ~25 kW/m and P_{max} of 45 kW/m at a burnup of ~100 MWh/kgU for intermediate-ring elements. The intermediate-ring elements subsequently achieved a burnup of ~400 MWh/kgU at a slowly declining power before the bundle was discharged. Intermediate-ring element 23 (hereafter E23) was selected for detailed characterization of the microchemistry at the fuel-sheath interface by imaging-XPS supported by SEM. Mass spectrometric analysis of the gas released upon puncture of the sheath (37.3 vol.% He, 7.97 vol.% Kr and 54.5 vol.% Xe) confirmed that this element had not failed.

Previously developed procedures that involve only dry-cutting operations were employed to obtain small samples from the sheath and both end caps [11]. Sheath samples were harvested in pairs, separated by 180° and facing toward or away from the bundle centre, at a distance of ~100 mm from either the bottom or the top (reference end) of the element. Axial locations corresponding to the approximate centre of the long axis of the sheath samples were intentionally chosen to coincide with likely pellet-pellet interfaces that had been identified by visual inspection. Following past practice, one sample was taken from near the centre of each end cap, but in addition, a second sample was cut from the periphery of the end cap. The latter included part of the sheath as well as the end cap and was intended to access the weld region between the sheath and the end cap. All of these samples were affixed, with conductive, silver-based epoxy, to stainless-steel foils that were then secured within a recessed area on a custom-designed sample-transfer mount. This arrangement minimizes the risk of spreading loose contamination from the sample to the instrument [11].

The active Imaging-XPS facility is based upon an ESCALAB 220i-XL instrument manufactured by VG Scientific; it incorporates a number of specialized modifications and custom-designed features for safe handling of highly radioactive materials [11]. Photoelectron emission was excited from the samples by a focussed beam of X-rays, with high spectral purity, produced by a monochromator that uses a pair of bent silicon crystals to filter Al Kα radiation ($h\nu = 1486.6$ eV). An X-ray spot size of ~500 μm was employed for all of the experiments conducted in the present study and the computer-controlled electron spectrometer, which consists of magnetic and electrostatic lenses and a concentric hemispherical analyser, was then used to further restrict the analysis area as required (~150 μm typically selected). An array of six channel electron multipliers provides high sensitivity and dynamic range for photoelectron spectroscopy, whereas a position-sensitive detector is employed for photoelectron imaging [11]. The spectrometer dispersion and work function were calibrated using gold, copper and silver standards with the binding-energy scale referenced to the Fermi level [11]. Static charging of the samples under the X-rays was usually minor, and any excess charge could also be neutralized by flooding the surface with low-energy electrons. An auxiliary Schottky field-emission electron gun, which is mounted directly on the instrument analysis chamber, provides *in situ* capabilities for scanning Auger microscopy (SAM) as well as SEM. The electron spectrometer is used for the former and a shielded secondary electron detector has been installed to facilitate the latter on radioactive materials. Precise alignment of the electron and X-ray beams at the focal point of the electron spectrometer was routinely checked using magnification and fluorescent standards.

Information on the near-surface composition as a function of depth was compiled by sequential XPS analysis and argon-ion sputter etching. A focussed 4 keV beam of Ar^+ at normal incidence, with a current of 1.3 μA, was rastered over the full area (~5 mm by ~7 mm) of the sample surface. Under these conditions, the sputter-etching rate has been determined to be ~0.5 nm/min using oxide thin-film standards [12]. An initial sputter of just 1 min was employed to remove any adventitious contamination (mainly adsorbed hydrocarbons and water from air-exposure) whilst minimizing any alteration of the original surface composition. All sputtering of fuel samples was performed in a custom-designed chamber that is isolated (beyond two gate valves) from the analysis chamber to avoid radioactive contamination of the sensitive detectors. The *in situ* SEM capability was essential for precisely locating the same features for XPS analysis after each ion-sputter interval.

After completion of the XPS analyses, the surface morphology of a number of samples was examined further using a shielded scanning electron microscope, which provided higher quality images than those obtained using the *in situ* SEM capability of the Imaging-XPS system. The microscope column of a JEOL 840A SEM has been mounted within a lead-shielded enclosure located above a hot cell to facilitate examination of highly radioactive materials. Provision of extended cables permitted the operator's console and electronics to be positioned outside the shielded enclosure.

3. Results

Secondary electron images collected (using the *in situ* SEM capability of the Imaging-XPS system) from a representative area and from a former pellet-pellet interface region on the inside surface of an E23 fuel-sheath sample are displayed in Fig. 1 in heat-scale pseudo-colour. A large patch of the CANLUB graphite coating (darker feature) that was retained on the surface can be distinguished from exposed sheath (lighter area) in Fig. 1(a), whereas the pellet-pellet interface area down the centre of Fig. 1(b) appears to be relatively clean.

Secondary electron images collected at a higher magnification (JEOL SEM) from representative areas, with and without a visible CANLUB layer, on an E23 fuel-sheath sample are reproduced in Fig. 2 using conventional grey scale. The very fine-grained and highly porous nature of the CANLUB graphite layer is illustrated in Fig. 2(a). As shown in Fig. 2(b), the surface of the exposed sheath often had a small amount of fine particulate debris and some graphite residues, although relatively clean areas were identified as well. Incipient axial cracks in the sheath surface (Fig. 2(b)) were commonly observed in areas without a visible retained CANLUB layer, especially at former pellet-pellet interface regions.

Representative XPS survey spectra that were recorded from regions with (Location #2) and without (Location #1) a visible retained CANLUB layer on the inside surface of an E23 fuel-sheath sample are compared in Fig. 3. Despite the pronounced differences in the appearance of the two areas, the C 1s peak is the most intense feature in both spectra. In other cases (with and without a CANLUB layer), the Cs 3d spin-orbit doublet was the dominant feature, followed by the O 1s peak and then the C 1s peak; however, quantitative analysis of the XPS data always confirmed that carbon was the most abundant species present at the surface. The zirconium emission features are noticeably more intense for the

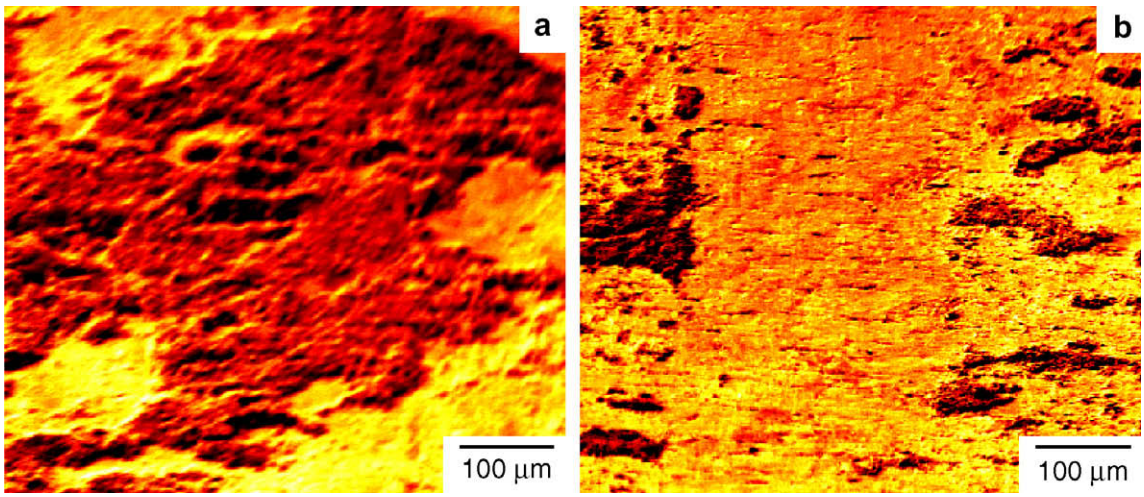

Fig. 1. Secondary electron images collected from the inside surface of an E23 fuel–sheath sample showing: (a) a large patch of the CANLUB coating, and (b) a former pellet–pellet interface area (down the centre of the image).

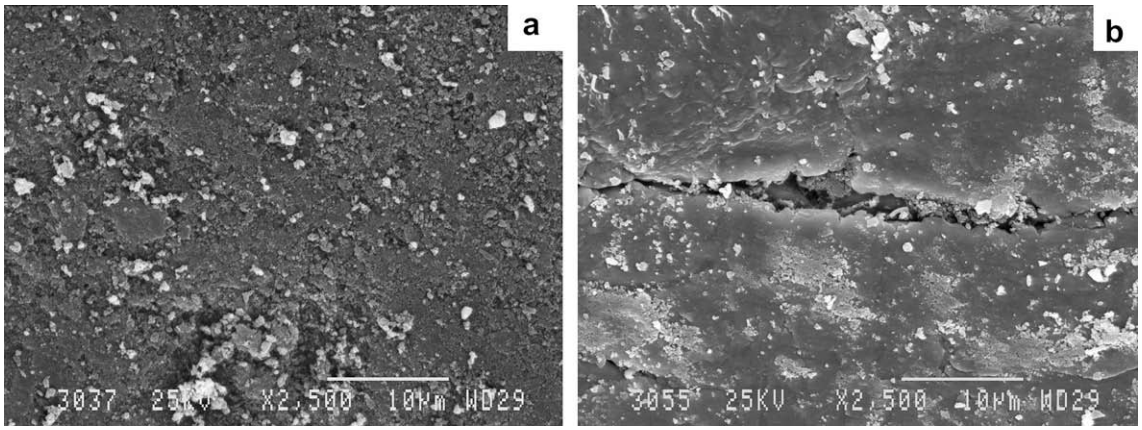

Fig. 2. Secondary electron images collected from representative areas on an E23 fuel–sheath sample: (a) with a dense retained CANLUB layer, and (b) without a visible CANLUB layer.

exposed-sheath location in Fig. 3, whereas weaker emission features assigned to uranium, barium, xenon, iodine, tin and rubidium have similar relative intensities in the two spectra.

Sequences of XPS spectra that were recorded from a visible CANLUB layer and from a relatively clean pellet-pellet interface region, after increasing intervals of argon-ion sputtering, have been reproduced in Figs. 4 and 5 respectively; similar results were obtained from comparable locations on other E23 fuel-sheath samples as well. In both figures, emission features arising from segregated fission products generally decrease following the longer sputter intervals; however, the rate of change also varies considerably (greatest for Cs and Rb, less for I and Xe, and least for Ba). Comparison of Figs. 4 and 5 indicates that all fission products decrease in abundance more slowly as a function of depth on the CANLUB layer than on the exposed sheath surface. The comparatively weak U 4f spin-orbit doublet shows some increase in strength over the first three sputter intervals before reaching a shallow maximum at about 60 min (both profiles). After the initial sputter, the C 1s peak increases in intensity, at both locations, thereafter remains almost constant to the end of the depth profile of the CANLUB layer, but decreases in strength beyond the 15 min sputter for the pellet-pellet interface region. Conversely, the zirconium emission features progressively increase in strength as a function of sputtering throughout the depth profile of the exposed sheath, whereas the weaker zirconium emission from the CANLUB layer shows only a minor increase after the initial few minutes of sputtering.

Although the C 1s emission features observed at locations with as well as without a visible CANLUB layer show some evidence of adventitious contamination before sputtering (asymmetry on the high binding energy side) the measured peak positions are still compatible with graphite [13]. After removal of the adventitious contamination by the initial sputter, both the shape and the position of the C 1s peak are characteristic of graphite for all locations. The development of a distinct shoulder on the low binding energy side of the C 1s emission toward the end of the depth profile on the pellet-pellet interface region (but not in Fig. 4) provides evidence of some carbide formation [13]. A broadened O 1s emission envelope (not shown), which could accommodate contributions from chemisorbed water, hydroxyl and carbonyl groups as well as oxides, was consistently observed for all samples before sputtering [13]. After sputtering, the O 1s emission collapsed into a relatively narrow and nearly symmetric peak, and the measured binding energies converged on a small range of values that are compatible with various oxides, including Cs_2O, UO_2 and ZrO_2 [13,14].

An overview of the inside surface of the weld between the fuel sheath and the end cap as well as the central area of the end cap at the top end of the E23 fuel element is provided by the secondary

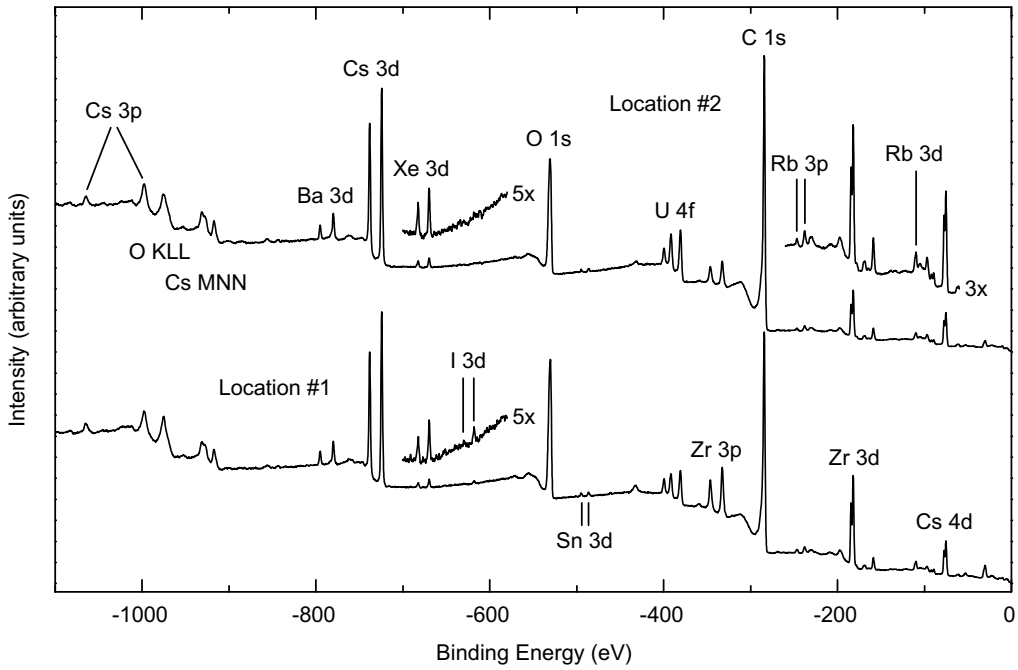

Fig. 3. Pair of XPS survey spectra recorded from different areas on an E23 fuel–sheath sample without (Location #1) and with (Location #2) a visible CANLUB layer.

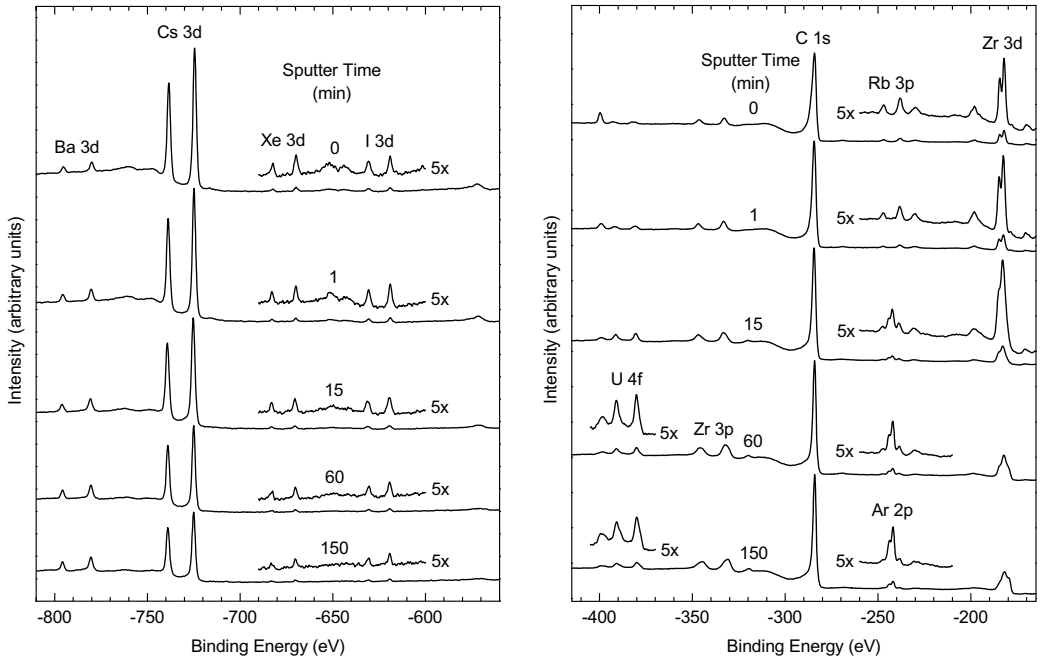

Fig. 4. Sequence of XPS spectra recorded from an area with a visible CANLUB layer on an E23 fuel–sheath sample, after increasing intervals of argon-ion sputtering.

electron images displayed in Fig. 6. Patches of the CANLUB layer that were retained on the sheath adjacent to the weld are also clearly visible in Fig. 6(a). The centre of the concave face of the end cap is located near the middle of Fig. 6(b) and some evidence of the original machining can still be identified. Aside from a few larger pieces of debris observed on the end cap, the textured surfaces of both the weld and the end cap are decorated by a very fine-grained deposit at low coverage (confirmed at higher magnification). The weld and the end cap at the bottom end of the E23 element were found to be more heavily coated with very fine-grained deposits, but not sufficiently to completely obscure the nodular texture of the underlying surfaces. Although the general appearance suggests deposits grown *in situ*, some contribution from debris produced during sample cutting cannot be excluded.

Representative XPS survey spectra that were recorded from the inside surface of the end-cap and the top of the weld (shown in Fig. 6) are compared in Fig. 7. Although there are some differences in the relative peak intensities, these spectra are quite similar, and consistent results were also obtained at other locations on both samples. In comparison with the exposed fuel sheath samples shown in Fig. 3, a richer surface chemistry of segregated fission products has been revealed here—including greater representation

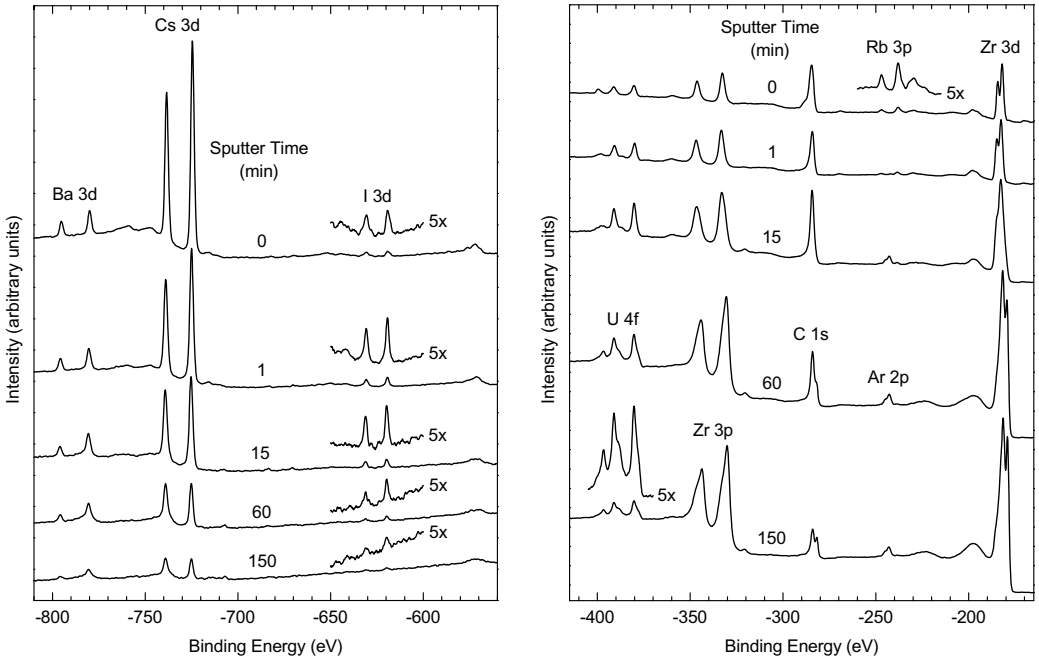

Fig. 5. Sequence of XPS spectra recorded from the pellet–pellet interface region on an E23 fuel–sheath sample (seen in Fig. 1(b)), after increasing intervals of argon-ion sputtering.

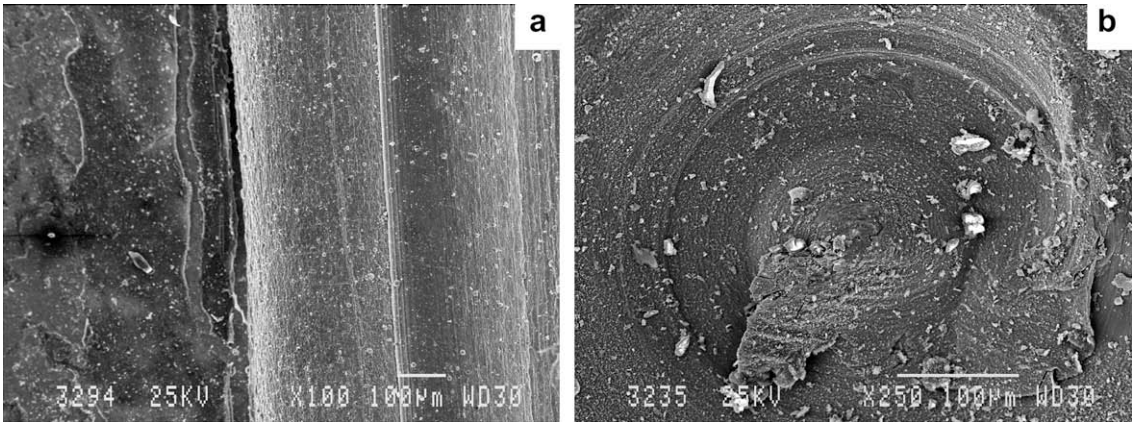

Fig. 6. Secondary electron images showing (a) the inside face of the weld between the fuel sheath and the end cap, and (b) the inside surface of the end cap, both from the top end of the E23 element.

from the less abundant fission products tellurium, iodine, cadmium, strontium and rubidium as well as high levels of cesium. The measured binding energies for the C 1s peak were again consistent with graphite, despite some evidence of an increase in the contribution from species with oxygen bonded to carbon (structure on the high binding energy side of the main peak) [13]. Comparable results were obtained from the bottom end of the E23 element (both end cap and weld), with the most notable difference being a modestly enhanced abundance of uranium relative to the segregated fission products.

Partial oxidation of uranium to the hexavalent state was indicated by the U $4f_{7/2}$ binding energies measured at all types of locations before sputtering [13,14]. On average, the degree of oxidation was greatest on the welds and least on the end caps with the fuel-sheath interface (both CANLUB layer and exposed sheath) at an intermediate level. Although the presence of cesium has been shown to promote the oxidation of uranium beyond the tetravalent state [14], only a weak correlation between the Cs/U ratio and the degree of oxidation was apparent here. The U $4f_{7/2}$ binding energies determined at all locations after argon-ion bombardment converge on the narrow range of values reported for stoichiometric UO_2 [13,14], which is consistent with the expected lack of fission-freed oxygen. As illustrated in Fig. 5, evidence of partial reduction of uranium to the elemental state (structure on the low binding energy side of both components of the U 4f spin-orbit doublet) was observed at several exposed sheath locations after extended sputtering. The binding energies measured for the Zr $3d_{5/2}$ core level on or near the surface of all samples were characteristic of the tetravalent state and typically in good agreement with the value expected for ZrO_2 [13]. Although some preferential sputtering (of oxygen) does occur from ZrO_2 under argon-ion bombardment [15], almost complete reduction to the elemental state was observed only toward the end of depth profiles at exposed sheath locations (Fig. 5). Recoil implantation of carbon and uranium by energetic fission fragments into the underlying sheath alloy could then potentially explain the evidence (discussed above) of carbide and

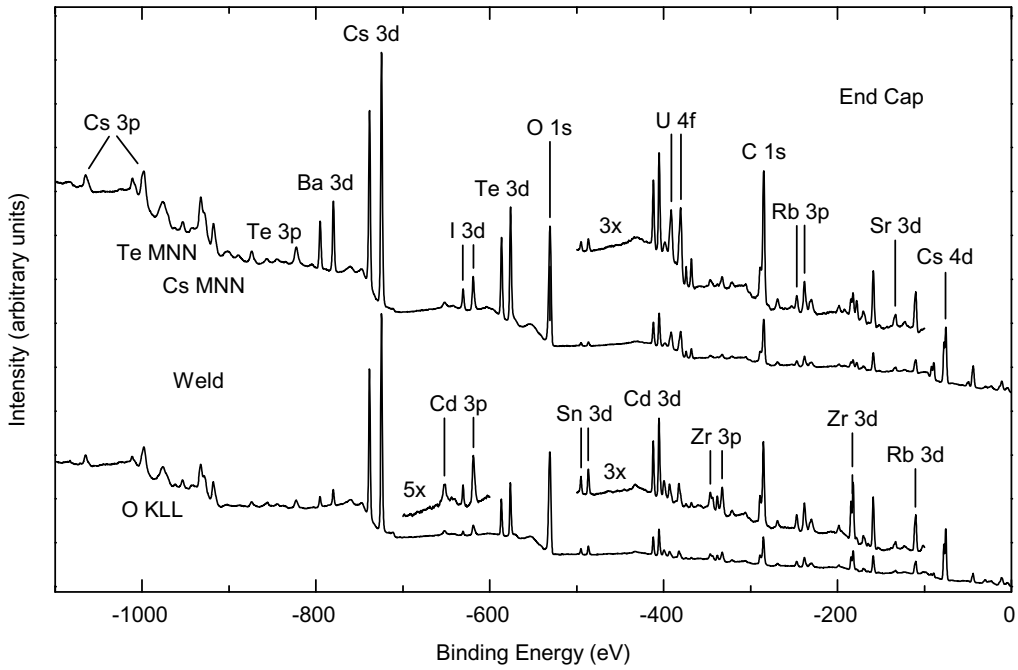

Fig. 7. Pair of XPS survey spectra recorded from the weld and the end cap on the top end of the E23 element (both shown in Fig. 6).

reduced uranium species toward the end of the same depth profiles.

The binding energies determined for the I $3d_{5/2}$ core level are compatible with a number of likely metallic iodides, including CsI and CdI_2 [13]. Although a +1 valence was clearly indicated by the chemical-shift data for cesium and rubidium, identification of specific compounds was not feasible [13]; however, formation of complex mixed oxides, halides and tellurides would seem probable. Both oxidized and reduced forms of tellurium were clearly identified on the E23 end-cap and weld samples, with the former predominant at the surface and the latter increasing as a function of argon-ion sputtering (depth profiles not shown). The binding energies measured for the Xe $3d_{5/2}$ core level at all fuel-sheath locations agreed well with the value (669.7 eV) reported for xenon absorbed in graphite [13]. Distinguishing between oxidized and reduced forms of strontium and barium by XPS is problematic, because of the small chemical-shifts involved, but only a +2 valence is plausible for either [13]. The measured Cd $3d_{5/2}$ binding energies, which decrease slightly after argon-ion sputtering, are compatible with elemental cadmium as well as a number of compounds, including $Cd(OH)_2$, CdTe, $CdCO_3$ and $CdTeO_3$ [13].

4. Discussion

The first stage in fission-product segregation and migration to the sheath is lattice diffusion to the grain boundaries, which is also normally the rate-determining step [4]. Thermal diffusion rates can be quite significant at the comparatively high temperatures [4–6] that are achieved near the centre-line of CANDU fuels under normal operating conditions. Further diffusion along the grain boundaries is presumed to be even more facile, and development of tunnels through inter-linkage of fission-gas bubbles on grain-boundary intersections can allow fast release of volatile fission products to the element void space [2–6]. Because of the steep radial temperature gradient in operating nuclear fuel, the key processes (lattice diffusion, grain boundary diffusion, and bubble formation and growth) are vastly more efficient near the pellet centre-line than toward its periphery [6]. The primary migration route for fission products should therefore be axially to the pellet end and then radially to the sheath—in the absence of large cracks that can provide a short-circuit pathway. A previous study of the microchemistry within standard CANDU fuel was entirely consistent with this scenario, with elevated levels of fission products found on the fuel-sheath interface only near former pellet-pellet interfaces [11]. Conversely, efficient infiltration of segregated fission products along the length of the sheath was observed for fuels that had experienced a significant power ramp or were irradiated to extended burnup (as in the present case) [16].

Detection of segregated fission products, especially cesium, at similar levels in the different types of sheath locations—with an intact CANLUB layer, with visible graphite residues and with only a thin film of carbon on otherwise exposed sheath—demonstrates effective infiltration across the full width of the graphite layer. The composition depth profiles also indicate that segregated fission products have migrated deep into the graphite grains at a microscopic level rather than just being adsorbed on their surfaces. These observations all support the hypothesis that the graphite must be effective at lowering the chemical activity of the segregated fission products rather than by providing an impervious barrier between the fuel and the sheath. The impact of the different conditions along the migration pathways has been manifested by the much richer fission-product chemistry on the end caps than the sheath; in particular, the greater abundance of barium and tellurium as well as the presence of strontium and noble metals. The composition on the weld surfaces was determined to be intermediate between that on the end caps and representative sheath areas, consistent with some lateral migration of fission products.

Migration of uranium oxide into and through the CANLUB layer, which has been consistently observed in studies of the microchemistry at the fuel-sheath interface including this one, can be attributed to severe radiation damage processes associated with fission occurring at the periphery of the fuel. Collision cascades that reach the pellet surface will cause recoil implantation of atoms and molecular fragments into the evolving interfacial layer, comprising segregated fission products, uranium oxide and graphite. Thermal-spike and pressure-gradient effects will also cause transient vaporization of fuel material at any location where a fission fragment

emerges from the pellet at high velocity. These energetic processes provide an explanation for the detection of elemental uranium and carbide below the zirconium oxide film at exposed sheath locations as well as the apparent migration of zirconia into the CANLUB layer. Variations in the composition across the fuel-CANLUB and CANLUB-sheath interfaces can be reasonably attributed to local differences in the density and thickness in the original graphite coating.

Severe radiation damage of the CANLUB layer by energetic fission fragments, supplemented by α-particles, β-particles, γ-rays and neutrons, will thus progressively occur during operation of the fuel in a reactor. Extensive disruption of the graphite sheets into smaller segments can be expected, whereas complete destruction of any residual organic binder seems assured. Introduction of segregated fission products and fragments of urania and zirconia with increasing burnup, through migration, recoil-implantation and thermal-spike effects, would further alter the properties of the evolving interfacial layer. The observation of a modest graphite contribution to the growing deposits on the end caps here, as well as in previous XPS studies of irradiated fuels, provides direct evidence of at least limited carbon mobility. This could be a key factor in the success of the CANLUB layer in protecting the sheath against attack by segregated fission products—allowing a thin film of graphite to be maintained on the entire sheath interior surface, despite formation of incipient cracks and other deformation processes. Migration of graphite away from the hottest zone near the fuel axis to cooler areas such as cracks in the periphery of pellets was observed in several historical graphite-disc fuels operated under severe conditions. The apparent disappearance of the CANLUB layer with extended burnup [9,10] can thus be attributed to a combination of relocation within the fuel element and physical loss of material during preparation of ceramographic cross-sections, because of degraded mechanical integrity, which should not interfere with its function as a fission-product chemical barrier during reactor operation.

5. Conclusions

The widespread distribution of segregated fission products, especially cesium, observed along the length of the E23 fuel sheath reflects the power history, which included a significant ramp early in life as well as irradiation to extended burnup. An even richer chemistry of segregated fission products was found on the end caps than on the sheath, with higher levels of barium, strontium, tellurium, iodine and cadmium relative to cesium. The intermediate composition measured on weld surfaces (between sheath and end caps) has been interpreted as indicating some lateral migration of fission products. These results are consistent with the premise that the primary migration route for fission products is along the hot central zone near the fuel centre line to the pellet end and then radially to the sheath followed by further spreading.

Secondary electron images collected from the E23 sheath samples illustrate well the fine-grained, porous nature of the CANLUB graphite layer. Effective infiltration of segregated fission products, especially cesium, across the full width of the graphite layer was demonstrated through a combination of microchemical XPS analyses at different sheath locations with varying degrees of CANLUB retention and composition depth profiling. These findings support the long-standing hypothesis that the graphite acts as a chemical rather than a physical barrier to segregated fission products. Severe radiation damage of the entire CANLUB layer, mainly by energetic fission fragments, will cause extensive disruption of the graphite sheets and complete destruction of any residual organic binder. Detection of graphite within the growing deposits on the end caps provides evidence of at least limited carbon mobility, which may be a key factor in maintaining dynamic protection of the sheath from localized attack by segregated fission products. Incorporation of urania and zirconia along with segregated fission products into the evolving interfacial layer between the sheath and the fuel can be explained by recoil implantation and thermal spike effects caused by energetic fission fragments.

Acknowledgements

The authors gratefully acknowledge the skilful work preformed by the Hot Cells staff at CRL, in particular R.C. Stothers and D.V. O'Brien, during preparation of fuel-sheath, weld and end-cap samples. They would also like to thank P.M. Ryan for operating the JOEL SEM.

References

[1] P.G. Boczar, in: D.B. Sanderson (Ed.), Proceedings of the Eighth International Conference CANDU Fuel, Honey Harbour, Ontario, CNS, Toronto, Canada, 2003, p. 36 (and AECL-CONF-1408).
[2] J.R. Matthews, J. Chem. Soc., Faraday Trans. 2 83 (1987) 1273.
[3] L.H. Johnson, D.W. Shoesmith, in: W. Lutze, R.C. Ewing (Eds.), Radioactive Waste Forms for the Future, Elsevier Science, Amsterdam, Netherlands, 1988, p. 635 (Chapter 11).
[4] J.H. Gittus, J.R. Matthews, P.E. Potter, J. Nucl. Mater. 166 (1989) 132.
[5] Hj. Matzke, J. Chem. Soc., Faraday Trans. 2 83 (1987) 1121.
[6] Hj. Matzke, Rad. Eff. 53 (1980) 219.
[7] H. Kleykamp, J. Nucl. Mater. 131 (1985) 221.
[8] B. Cox, J. Nucl. Mater. 172 (1990) 249.
[9] M.R. Floyd, J. Novak, P.T. Truant, Fission-gas release in fuel performing to extended burnups in Ontario hydro nuclear generating stations. AECL Report, AECL-10636, 1992.
[10] M.R. Floyd, in: B.J. Lewis (Ed.), Proceedings of the Seventh International Conference CANDU Fuel, vol. 2, Kingston, Ontario, CNS, Toronto, Canada, 2001, p. 5A1 (and AECL-CONF-1135).
[11] W.H. Hocking, K.G. Irving, in: B.J. Lewis (Ed.), Proceedings of the Seventh International Conference CANDU Fuel, vol. 1, Kingston, Ontario, CNS, Toronto, Canada, 2001, p. 163 (and AECL-12135).
[12] W.H. Hocking, R.A. Verrall, P.G. Lucuta, Hj. Matzke, Radiat. Eff. Defects Solids 125 (1993) 299.
[13] J.F. Moulder, W.F. Stickle, P.E. Sobol, K.D. Bomben, in: J. Chastain, R.C. King Jr. (Eds.), Handbook of X-ray Photoelectron Spectroscopy, Physical Electronics, Eden Prairie, USA, 1995.
[14] S. Van den Berghe, F. Miserque, T. Gouder, B. Gaudreau, M. Verwerft, J. Nucl. Mater. 294 (2001) 168.
[15] D.F. Mitchell, G.I. Sproule, M.J. Graham, Surf. Interface Anal. 15 (1990) 487.
[16] W.H. Hocking, K.G. Irving, T. Do, in: D.B. Sanderson (Ed.), Proceedings of the Eighth International Conference CANDU Fuel, Honey Harbour, Ontario, CNS, Toronto, Canada, 2003, p. 75 (and AECL-CONF-1350).